Proc. Schl. Eng. Tokai Univ., Ser. E
43 (2018) 38-45

Influence of Radiation Impedance on Energy Recovery Characteristics of Electricity Generation System with Piezoelectric Element

by

Hiroyuki MORIYAMA[*1], Yuto OHBA[*2] and Hirotarou TSUCHIYA[*3]

(Received on Apr. 2, 2018 and accepted on Jul. 5, 2018)

Abstract

This paper describes the electricity generation characteristics of a new energy-harvesting system with piezoelectric elements. The proposed system is composed of a cylinder and thin plates at both ends. The piezoelectric elements are installed at the centers of both plates, and one side of each plate is subjected to a harmonic point force. In this system, vibration energy is converted into electrical energy via electro-mechanical coupling between the plate vibration and piezoelectric effect. In addition, the acoustic energy radiated from the plate induces a self-sustained vibration at the other plate via mechanical-acoustic coupling between the plate vibrations and an internal sound field into the cylindrical enclosure. Therefore, the electricity generation characteristics should be considered as an electro-mechanical-acoustic coupling problem. The characteristics are estimated theoretically and experimentally from the electric power in the electricity generation, the mechanical power supplied to the plate and the electricity generation efficiency that is derived from the ratio of both types of power. In particular, the electricity generation efficiency is one of the most appropriate factors to evaluate the performance of electricity generation systems. Thus, the effect of mechanical-acoustic coupling is principally evaluated by examining the electricity generation efficiency.

Keywords: Electricity generation system, Piezoelectric element, Radiation impedance

1. Introduction

Scavenging untapped vibration energy by converting into it usable electric energy via piezoelectric materials has attracted considerable attention and has been regarded as one of new energy sources[1)]. Typical energy harvesters adopt a simple cantilever configuration to generate electric energy via piezoelectric materials, which are attached to or embedded in host structures, and the behavior is governed by electro-mechanical coupling phenomena.

To improve the conversion efficiency, a mechanical impedance matching method, which was derived from using spacers between the piezoelectric element and beam structure and tuning for the size of the piezoelectric element, was proposed[2)]. These structural vibrations are caused by vibrators and various power sources. For instance, a self-sustained oscillation caused by placing a plate into a flow whose critical velocity was overpassed (so-called ‘fluttering’) is a well-known phenomenon. To utilize such a fluttering phenomenon for energy-harvesting, the plate on which the piezoelectric elements were arranged was used, and the effect of their arrangement along the flow axis was considered. Then an optimization of the arrangement was performed among some positions and dimensions of piezoelectric elements[3)].

In this study, a circular plate, on which a piezoelectric element is installed at its center, is adopted as the host structure in consideration of future versatility and is subjected to a harmonic point force. Because the acoustic radiation of circular plate is better than that of beam structure, harvesting acoustic energy radiated from the structure is one of important matters to improve electricity generation characteristics. Hence, a cylinder with the above plates at both ends is used, and mechanical-acoustic coupling between the plate vibra-tions and internal sound field is applied to the electricity generation[4-6)]. Consequently, the electro-mechanical-acoustic coupling problem must be considered and is estimated theoretically and experimentally from the electric power caused by the electricity generation, the mechanical power

*1 Professor, Department of Prime Mover Engineering
*2 Graduate Student, Course of Mechanical Engineering
*3 Lecturer, Department of Precision Engineering

supplied to the plate, and the electricity generation efficiency that is derived from the ratio of both powers. In particular, by focusing on the electricity generation efficiency as the most significant characteristic, we verify that the performance of the proposed system is improved by using mechanical-acoustic coupling in comparison with using only the plate vibration without coupling.

2. Analytical method

2.1 *Analytical model*

The analytical model consists of a cavity with two circular end plates, as shown in Fig. 1. Plates 1 and 2 are supported by translational and rotational springs distributed at constant intervals and the support conditions are determined by the translational spring stiffnesses T and the rotational spring stiffnesses R. The plates of radius r_c have a Young's modulus E_c and a Poisson's ratio ν_c, however, the plate thickness is denoted by h_{c1} and h_{c2}, because it's possible the plates are different in the thickness. On the surfaces of both plates, piezoelectric elements are installed at the centers of the plates and have radius r_p, thickness h_p, Young's modulus E_p, and Poisson's ratio ν_p. Then an electrode plate is sandwiched between the above plate and piezoelectric element and has radius r_b, thickness h_b, Young's modulus E_b and Poisson's ratio ν_b. The suffixes c, p and b herein indicate the circular plate, piezoelectric element and electrode plate. On the other hand, the sound field, which is assumed to be cylindrical, has the same radius as that of the plates and varying length L because the resonance frequency depends on the length. The boundary conditions are considered structurally and acoustically rigid at the lateral wall between the structure and sound field. The coordinates used are radius r, angle ϕ between the planes of the plates and the cross-sectional plane of the cavity and distance z along the cylinder axis. The periodic point force F is applied to plate 1 at distance r_1 and angle ϕ_1. The natural frequency of the plates is employed as the excitation frequency.

w_{c1} and w_{c2} are the flexural displacements of the plates, w_{p1} and w_{p2} are those of the piezoelectric elements installed on the plates, and the suffixes 1 and 2 indicate plates 1 and 2, respectively. They are found by substituting X^{s}_{nm} of Eq. (2) for the plate modes into Eq. (1) as suitable trial functions. The flexural displacements of the piezoelectric elements are identical to those of the plates, respectively, because it is assumed that the piezoelectric elements adhere completely to each circular plate through the electrode plate.

$$\left.\begin{aligned} w_{c1} = w_{p1} = \sum_{s=0}^{1}\sum_{n=0}^{\infty}\sum_{m=0}^{\infty} X^s_{nm} A^s_{1nm}\, \mathrm{e}^{\mathrm{j}(\omega t+\alpha_1)}, \\ w_{c2} = w_{p2} = \sum_{s=0}^{1}\sum_{n=0}^{\infty}\sum_{m=0}^{\infty} X^s_{nm} A^s_{2nm}\, \mathrm{e}^{\mathrm{j}(\omega t+\alpha_2)}, \end{aligned}\right\} \quad (1)$$

$$X^s_{nm} = \sin(n\phi + s\pi/2)\,(r/r_c)^m, \quad (2)$$

where n, m and s are, respectively, the circumferential order, radial order and symmetry index with respect to the plate vibration. A^s_{1nm} and A^s_{2nm} are coefficients to be determined, ω is the angular frequency of the harmonic point force acting on the plate, and t is the elapsed time. α_1 and α_2 are the phases of the respective plate vibrations. In this analysis, α_1 is set to 0°, and α_2 ranges from 0° to 180°.

2.2 *Modelling of Piezoelectric Part*

Only the piezoelectric part of plate 1 is used to explain its modelling in this section. The relationships of stress σ_{p1}, strain ε_{p1}, electric displacement D_1, and electric field E_1 are as follows:

$$\begin{Bmatrix} \sigma_{p1} \\ D_1 \end{Bmatrix} = \begin{bmatrix} E_p^E & -e^T \\ e & \gamma^\varepsilon \end{bmatrix} \begin{Bmatrix} \varepsilon_{p1} \\ E_1 \end{Bmatrix}. \quad (3)$$

E_p^E signifies Young's modulus that was measured at a constant electric field, and γ^ε indicates the dielectric constant that was measured at a constant strain. The above equation expresses relationships between electrical and mechanical characteristics of a piezoelectric element, and the stress is concretely related to the electric field by the piezoelectric coupling coefficient e. The piezoelectric coupling coefficient is expressed as

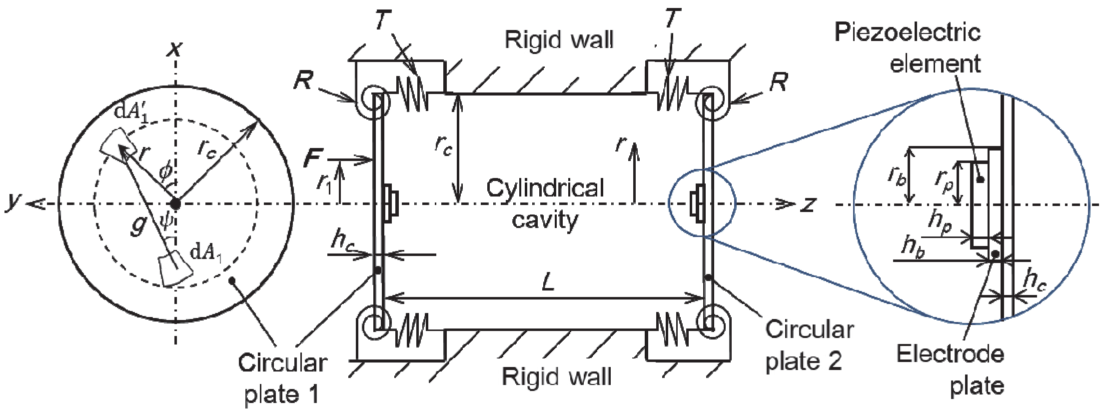

Fig. 1 Configuration of analytical model.

$$e = d_{31}E_P^E, \tag{4}$$

where d_{31} is the piezoelectric strain constant, in which the electric field occurs in the normal direction of the in-plane strain.

Then the electric field E_1, which occurs between both sides of the piezoelectric element, is expressed as follows:

$$E_1 = Y_{nm}v_1 = -R_p\dot{q}_1 = \mathrm{j}\omega B_{1nm}^s e^{\mathrm{j}(\omega t+\alpha_1)}. \tag{5}$$

v_1 is the voltage that occurs in the electric field. We assume that the electric potential across the piezoelectric element is constant, since it is in the field that is not applied to the plate. Thus, Y_{nm} is defined as described above. R_p is the overall resistance value in an electricity generation circuit. The magnitude of the electric charge q_1 depends on the coefficient B^s_{1nm} that is determined in this analysis as with A^s_{1nm}.

$$Y_{nm} = \begin{cases} -1/h_p & h_c/2 < z < h_c/2 + h_b + h_p, \\ 0 & h_c/2 < z < h_c/2 + h_b + h_p, \end{cases} \tag{6}$$

$$q_1 = B_{1nm}^s e^{\mathrm{j}(\omega t+\alpha_1)}. \tag{7}$$

In order to easily express the electro-mechanical equation, the elements $M^s_{p1nmm'}$ and $K^s_{p1nmm'}$ of the mass and stiffness matrices can be denoted as

$$M_{p1nmm'}^s = \int_{V_{p1}} \rho_p X_{nm}^s X_{nm'}^s \mathrm{d}V_{p1}, \tag{8}$$

$$K_{p1nmm'}^s = \int_{V_{p1}} z^2 X_{nm}^{s\,''} E_p^E X_{nm'}^{s\,''} \mathrm{d}V_{p1}. \tag{9}$$

The index m' is also of a radial order and has a transposed relation to m. The elements θ_1 and C_{p1} of the electro-mechanical coupling and capacitance matrices are defined as

$$\theta_1 = -\int_{V_{p1}} z\rho_p X_{nm}^s e Y_{nm'} \mathrm{d}V_{p1}, \tag{10}$$

$$C_{p1} = \int_{V_{p1}} Y_{nm} \gamma^\varepsilon Y_{nm'}^s \mathrm{d}V_{p1}. \tag{11}$$

2.3 *Governing equations of electro-mechanical-acoustic coupling*

Here, electro-mechanical coupling is considered from the above several relationships, and then mechanical-acoustic coupling is also taken based on the relationships between the vibrations of both plates and the sound field into the cylindrical enclosure. As a result, this electricity generation phenomenon depends strongly on electro-mechanical-acoustic coupling, so that the motions of both plates having a piezoelectric part are governed by the following Eqs. (12) and (13), respectively:

$$\sum_{m'=0}^{\infty} \Big[\big\{K_{c1nmm'}^s(1+\mathrm{j}\eta_c) + K_{p1nmm'}^s(1+\mathrm{j}\eta_p) + K_{b1nmm'}^s \times (1+\mathrm{j}\eta_b) - \omega^2\big(M_{c1nmm'}^s + M_{p1nmm'}^s + M_{b1nmm'}^s\big) + r_c F_{sn}\Big\{T + \Big(\frac{m}{r_c}\Big)\Big(\frac{m'}{r_c}\Big)R\Big\}\Big] A_{1nm'}^s e^{\mathrm{j}\alpha_1} - \sum_{m'=0}^{\infty} \theta_1 v B_{1nm'}^s e^{\mathrm{j}\alpha_1} = \mathbf{F}_{nm}^s e^{\mathrm{j}\alpha_1} - \mathbf{S}_{1nm}^s \tag{12}$$

$$\sum_{m'=0}^{\infty} \Big[\big\{K_{c2nmm'}^s(1+\mathrm{j}\eta_c) + K_{p2nmm'}^s(1+\mathrm{j}\eta_p) + K_{b2nmm'}^s \times (1+\mathrm{j}\eta_b) - \omega^2\big(M_{c2nmm'}^s + M_{p2nmm'}^s + M_{b2nmm'}^s\big) + r_c F_{sn}\Big\{T + \Big(\frac{m}{r_c}\Big)\Big(\frac{m'}{r_c}\Big)R\Big\}\Big] A_{2nm'}^s e^{\mathrm{j}\alpha_2} - \sum_{m'=0}^{\infty} \theta_2 v B_{2nm'}^s e^{\mathrm{j}\alpha_2} = \mathbf{S}_{2nm}^s \tag{13}$$

$K^s_{c1nmm'}$, $K^s_{b1nmm'}$ and $K^s_{c2nmm'}$, $K^s_{b2nmm'}$ are stiffness matrix elements and $M^s_{c1nmm'}$, $M^s_{b1nmm'}$ and $M^s_{c2nmm'}$, $M^s_{b2nmm'}$ are mass matrix elements with respect to the circular and electrode plates, respectively. These are elements of the symmetrical matrices, because the index m' has a transposed relation to m, as with $M^s_{p1nmm'}$ and $K^s_{p1nmm'}$. η_c, η_p and η_b are the structural damping factors of the circular plate, piezoelectric element and electrode plate, respectively. Moreover, F_{sn} is a coefficient that is determined by the indices n and s, $\mathbf{F}^s_{nm}$ is a load vector that expresses the point force on plate 1, and $\mathbf{S}^s_{nm1}$ and $\mathbf{S}^s_{nm2}$ are the acoustic excitation vectors that express the acoustic excitations of both plates. The details of F_{sn} and the elements F^s_{nm}, S^s_{nm1} and S^s_{nm2} of the respective vectors are as follows:

$$F_{sn} = \begin{cases} \pi, \text{at } n \neq 0, \\ 0, \text{at } n = 0 \text{ and } s = 0, \\ 2\pi, \text{at } n = 0 \text{ and } s = 1, \end{cases} \tag{14}$$

$$F_{sn} = \int_{A_1} F\delta(r - r_1)\delta(\phi - \phi_1)\,\mathrm{d}A_1, \tag{15}$$

$$S_{1nm}^s = \int_{A_1} P_s X_{nm}^s\,\mathrm{d}A_1,\ S_{2nm}^s = \int_{A_2} P_s X_{nm}^s\,\mathrm{d}A_2. \tag{16}$$

Here, δ is the delta function associated with the point force on plate 1, whose area is denoted by A_1. P_s is the sound pressure at an arbitrary point on the boundary surface of the plates, and A_2 signifies the area of plate 2.

On the other hand, the electricity generation behaviors of these piezoelectric elements are governed by the following Eqs. (17) and (18), respectively:

$$\sum_{m'=0}^{\infty} C_{p1}^{-1}\theta_1 A_{1nm'}^s = \sum_{m'=0}^{\infty} \big(\mathrm{j}\omega R_p + C_{p1}^{-1}\big) B_{1nm'}^s, \tag{17}$$

$$\sum_{m'=0}^{\infty} C_{p2}^{-1}\theta_2 A_{2nm'}^s = \sum_{m'=0}^{\infty} \big(\mathrm{j}\omega R_p + C_{p2}^{-1}\big) B_{2nm'}^s. \tag{18}$$

In actual calculation, the relationships between $A^s{}_{1nm}$ and $B^s{}_{1nm}$ and between $A^s{}_{2nm}$ and $B^s{}_{2nm}$ are obtained from Eqs. (18) and (19), and they are applied to Eqs.(12) and (13), respectively, with the result that $A^s{}_{1nm}$, $A^s{}_{2nm}$, $B^s{}_{1nm}$ and $B^s{}_{2nm}$ can be derived by solving the above simultaneous equations (12) and (13).

2.4 *Radiation impedance of circular plate*

A radiation impedance of circular plate is taken up in this section. To simplify the problem, it is assumed that the acoustic radiation is caused by a circular piston source, in which plate 1 has the velocity amplitude U_0. With respect to minute areas $\mathrm{d}A_1'$ and $\mathrm{d}A_1$ in Fig. 1, the sound pressure P_s at $\mathrm{d}A_1'$, which is derived from the mechanical motion of an arbitrary area $\mathrm{d}A_1$, is defined as follows[5]:

$$P_s = \int_{A_1} \frac{\mathrm{j}\rho_a ck}{2\pi g} U_0 \mathrm{e}^{\mathrm{j}(\omega t - kg)} \mathrm{d}A_1, \tag{19}$$

where ρ_a and c are the fluid density and speed of sound in the cavity, respectively, k is the wavelength constant, and g is the distance between $\mathrm{d}A_1'$ and $\mathrm{d}A_1$ on plate 1.

The reaction force F_r against the above the sound pressure on plate 1 can be calculated from the following equation.

$$F_r = \int_{A_1} P_s\, \mathrm{d}A_1' = \frac{\mathrm{j}\rho_a ck}{2\pi g} U_0 \mathrm{e}^{\mathrm{j}\omega t} \int_{A_1} \mathrm{d}A_1' \int_{A_1} \frac{\mathrm{e}^{-\mathrm{j}kg}}{g} \mathrm{d}A_1. \tag{20}$$

The above equation is rewritten from the relationship between $\mathrm{d}A_1'$ and $\mathrm{d}A_1$.

$$F_r = \frac{\mathrm{j}\rho_a ck}{\pi} U_0 \mathrm{e}^{\mathrm{j}\omega t} \int_0^{r_c} r\mathrm{d}r \int_0^{2\pi} \mathrm{d}\phi \int_{-\frac{\pi}{2}}^{\frac{\pi}{2}} d\psi \int_0^{2r\cos\psi} \mathrm{e}^{-\mathrm{j}kg}\, dg$$

$$= Z_r U_0 \mathrm{e}^{\mathrm{j}\omega t} = (R_r + \mathrm{j}X_r) U_0 \mathrm{e}^{\mathrm{j}\omega t}, \tag{21}$$

where Z_r is radiation impedance and is constructed of radiation resistance R_r of the real part and radiation reactance X_r of the imaginary part. Then the detailes of normalized R_{rn} and X_{rn} are as follows:

$$R_{rn} = \frac{R_r}{\rho_a c\pi r_c^2} = \frac{(2kr_c)^2}{2\cdot 4} - \frac{(2kr_c)^4}{2\cdot 4^2\cdot 6} + \frac{(2kr_c)^6}{2\cdot 4^2\cdot 6^2\cdot 8} - \cdots, \tag{22}$$

$$X_{rn} = \frac{X_r}{\rho_a c\pi r_c^2} = \frac{4}{\pi}\left\{\frac{2kr_c}{3} - \frac{(2kr_c)^3}{3^2\cdot 5} + \frac{(2kr_c)^5}{3^2\cdot 5^2\cdot 7} - \cdots\right\}. \tag{23}$$

3. Experimental apparatus and method

Figs. 2(a) shows the configuration of the experimental apparatus used in this study. The structure consists of a steel cylinder with circular aluminum end plates. The radius r_c of end plates is 153 mm and is the same as the inner radius of cylinder. Then the thickness h_c adopts 2.0, 2.5, 3.0 and 4.0 mm and the length L of cylinder can range from 500 to 2000 mm to emulate the analytical model. Plate 1 is subjected to the point force excited by a small vibrator. The excitation is carried out near the natural frequency of the (0,0) mode. The position of the point force r_1 is normalized by radius r_c and is set to $r_1/ r_c = 0.4$.

To estimate the mechanical power P_m supplied to plate 1 by the small vibrator, an acceleration sensor is installed near the position of the point force on plate 1, and P_m is predicted from the point force and acceleration a_1. The phase difference between the plate vibrations is also measured owing to the installation of the acceleration sensor at the same position on plate 2, resulting in significant effects on the mechanical-acoustic coupling. To estimate the internal acoustic characteristics, the sound pressure level in the cavity is measured using condenser microphones with a probe tube. The tips of the probe tubes are located near the plates and the cylinder wall, which are the approximate locations of the maximum sound pressure level when the sound field becomes resonant.

To perform the electricity generation experiment, the piezoelectric element is used. It is comprised of a piezoelectric part constructed of ceramics and an electrode part constructed of brass, which have radiuses r_p and r_b of 12.5 and 17.5 mm and thicknesses h_p and h_b of 0.23 and 0.30 mm, respectively. The piezoelectric elements are installed at the centers of both plates. The electric power P_e generated by the expansion and contraction of the piezoelectric elements on plates 1 and 2 are discharged through the resistance circuit, which consists of three resistors having resistances R_v, R_i and R_c, as shown in Fig. 2(b). R_v and R_i are the resistances of the voltmeter and ammeter, which are built-into the wattmeter, and are 2 MΩ and 2 mΩ, respectively; while R_c is the resistance of the resistor connected outside the wattmeter and is 97.5 kΩ. To grasp the effect of mechanical-acoustic coupling on energy harvesting, the electric power and other data are also measured without the cylinder (i.e. in the electricity generation under the vibration of only plate 1) and are estimated in comparison with those with cylinder.

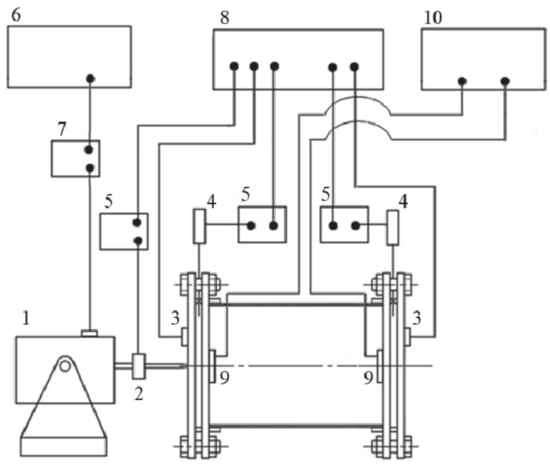

1: Vibration generator, 2: Load cell, 3: Acceleration sensor, 4: Condenser microphone, 5: Amplifier, 6: Multifunction generator, 7: Power supply, 8: FFT analyzer, 9: Piezoelectric element, 10: Power meter

(a) Measurement system.

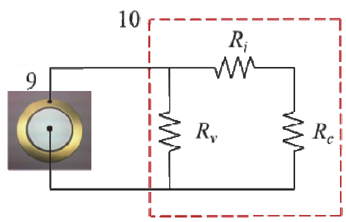

(b) Electrical circuit of energy-harvesting device.

Fig. 2 Configuration of experimental apparatus.

4. Results and discussion

4.1 *Vibration and electricity generation characteristics of only plate*

In the theoretical study, the plates are assumed to be aluminum having a Young's modulus E of 71 GPa and a Poisson's ratio ν of 0.33. The plate radius r_c are constant at 153 mm and the plate thickness h_c ranges from 1.5 mm to 4.5 mm. The support conditions of the plates, which have flexural rigidity D [$= Eh_c^3/\{12(1-\nu^2)\}$], are expressed by the non-dimensional stiffness parameters T_n ($= Tr_c^3/D$) and R_n ($= Rr_c/D$). These values are identical for both plates. If R_n ranges from 0 to 10^8 when T_n is 10^8, the support condition can be assumed from a simple support to a clamped support. The actual condition adopts $T_n = 10^8$ $R_n = 10^1$ to get closer to the experimental support condition. Plate 1 is subjected to the point forces F_1, which are set to 1 N and are located at $r_1/r_c = 0.4$, as with the actual excitation experiment.

With respect to the electricity generation system of only plate 1 reduced the cylinder and plate 2 in Fig. 1, Fig. 3 shows the flexural displacement at the excitation point as functions of the excitation frequency in the theoretical results, when the plate thickness h_c = 2.0, 2.5, 3.0 and 4.0 mm. However, the displacement w_{c1} is indicated by the root-mean-squear value w_{1rms}. w_{1rms} reaches a peak in the vicinities of the respective natural frequencies of plate 1 and tends to be decreased by thickening. Taking note of natural frequency and flexural displacement of a circular plate, they depend on the flexural rigidity D according to the classical theory. Specifically, the natural frequency and flexural displacement are proportional to $D^{0.5}$ and D^{-1}, respectively, so that the displacement is affected more strongly by changing h_c than the natural frequency. The displacement behavior causes the electricity generation voltage v_1 of the piezoelectric element attached on plate 1 and the root-mean-square v_{1rms} is indicated in Fig. 4 in the same manner of Fig. 3. v_{1rms} behaves in a similar manner to w_{1rms} in occurrences of peaks and variations in peak values with changing h_c.

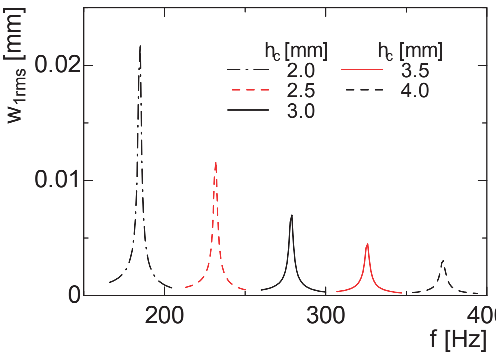

Fig. 3 Flexural displacement at excitation point as function of excitation frequency.

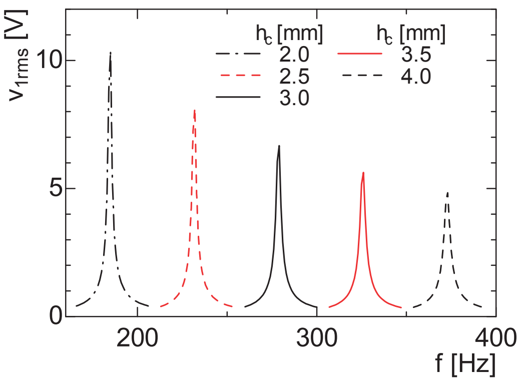

Fig. 4 Voltage with electricity generation as function of excitation frequency.

Here, the power P_m supplied from the vibrator is calculated from the product between F and w_{c1}. Fig. 5 shows the theoretical supplied power P_m as a function of h_c. P_m decreases gradually with increasing h_c, whereas its variation is somewhat extreme in comparison with that of w_{1rms}. This is because w_{c1} is proportional to F, with the result that P_m is proportional to the square of w_{c1}. On the other hand, the electric power P_e at the electricity generation is also exhibited in the same figure. P_e has behavior similar to P_m, since v_1 has strong correlation to w_{c1}. Because the piezoelectric element is assumed to be incorporated in the electrical circuit of energy-harvesting device and to be connected in series with the resistance for power consumption, it is natural that an electrical current is in-phase to the voltage. Therefore, because P_e is proportional to the square of v_1, its variation becomes somewhat extreme in comparison with that of v_1 as with the relationship between P_m and w_{c1}.

4.2 *Improvement electricity generation characteristics*

In this section, to improve electricity generation characteristics by means of using mechanical-acoustic coupling, the cylinder and plate 2 are added to the above plate 1, as shown in Fig. 1. The supplied power P_m and the electric power P_e are also calculated in the analytical model using the cylindrical structure whose radius is constant at 153 mm, whereas the length L of the cylindrical sound field having the

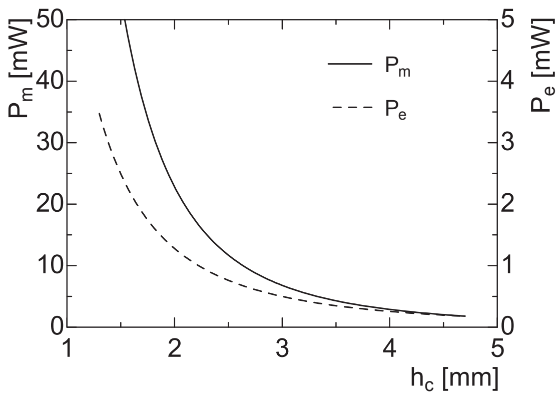

Fig. 5 Supplied and electric powers as function of plate thickness.

same radius as that of the plates varies from 100 to 2000 mm. Fig. 6 shows P_m as a function of h_c together with the results of only plate 1. However, P_m at the specific L, at which P_e is maximized, is exhibited as the data using coupling. P_m decreases gradually with increasing h_c in similar manner to that of only plate 1, while the values are considerably less than that of only plate 1. Although plate 1 is subjected to the point force of 1 N in both cases, the power derived from the force is almost spent to the vibration of plate 1 without coupling, i.e. only plate. On the other hand, the power is spent to not only forming the internal sound field but also vibrating plate 2 with coupling. In other words, the formation of the sound field behaves as a resistance against the vibration of plate 1, so that the flexural displacement w_{c1} is suppressed and P_m is decreased in comparison with that without coupling.

Fig. 7 shows P_e corresponding to the above P_m as a function of h_c together with the results of only plate 1. Naturally, P_e also decreases with increasing h_c and is less than that of only plate 1. By the way, Fig. 8 shows the sound pressure level L_{pv}, L_{p1} and L_{p2} as functions of L. The theoretical level L_{pv} is averaged over the entire volume of the cavity and is maximized at each L, when h_c and f are set to 3 mm and 280 Hz and the phase α_2 ranges from 0 to 180°. The theoretical level L_{pv} peaks at 610, 1230 and 1840 mm. The peaks are caused by the promotion of mechanical-acoustic coupling between the plate vibration and acoustic modes. Then the acoustic modes are the (0,0,1), (0,0,2) and (0,0,3) modes whose plane modal shape is similar to that of plate vibration mode (0,0). The experimental levels L_{p1} and L_{p2}, which are measured near plates 1 and 2, correspond to L_{pv} in the occurrence of those peaks, so that it is obvious to promote coupling around the above lengths. These P_m and P_e with coupling are the results under such a situation that involves with the (0,0,1) mode.

A close relationship between P_m and P_e can be confirmed from these results. In addition, to consider concretely this relationship, the electricity generation efficiency P_{em} is defined as follows:

$$P_{em} = \frac{P_e}{P_m} \times 100\ [\%]\,. \tag{24}$$

Fig. 9 shows P_{em} derived from the above P_m and P_e as a function of h_c, then not only theoretical but also experimental P_{em} is indicated. In the case of only plate 1, theoretical P_{em} increases gradually with increasing h_c, whereas the experimental P_{em} presents a totally reverse tendency where it decreases gradually with increasing h_c. On the other hand, in the case where coupling is used, theoretical P_{em} also increases gradually with increasing h_c and is very close to that of only plate 1. Furthermore, the experimental P_{em} corresponds to the theoretical results and the discrepancy between the theoretical and experimental data cannot be recognized as with that of only plate 1.

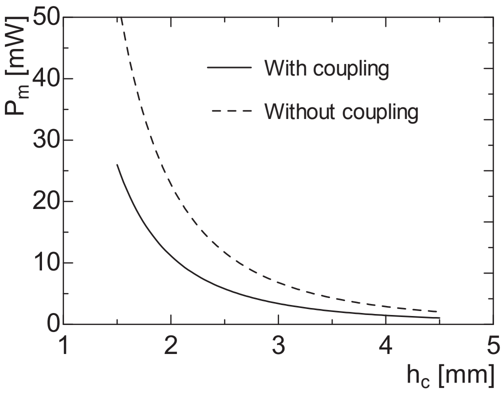

Fig. 6 Supplied power as function of plate thickness.

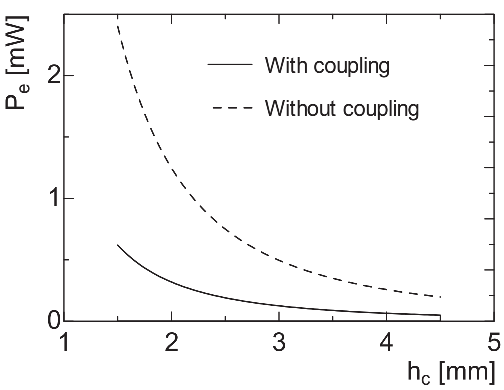

Fig. 7 Electric power as function of plate thickness.

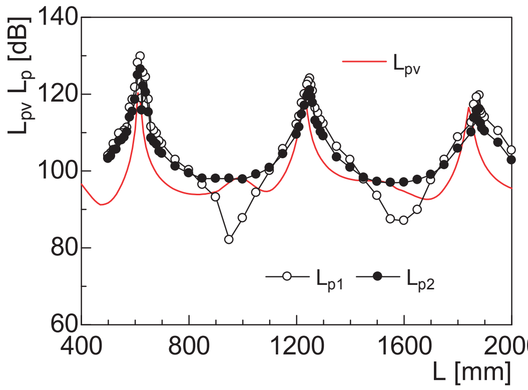

Fig. 8 Sound pressure level as function of cylinder length

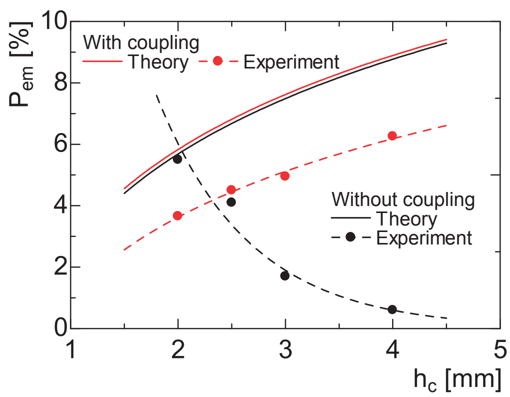

Fig. 9 Electricity generation efficiency as function of plate thickness.

In the analytical model of only plate 1, the medium contacted on plate 1 is not assumed, i.e. there is plate 1 in vacuo. Therefore, the radiated sound field is not formed by the vibration of plate 1 and the acoustic radiation power is almost spent to the electricity generation, so that it is supposed that the above discrepancy took place since the actual vibration of plate 1 forms the sound field. However, because the vibration of plate 1 contributes to the formation of the internal sound field and the vibration of plate 2 in the analytical model having the cylindrical structure, it is supposed that such a discrepancy did not take place like the case of only plate 1.

4.3 *Influence of radiation impedance on electricity generation*

As mentioned in Section 2.4, the radiation impedance Z_r consists of the radiation resistance R_r of its real part and the radiation reactance X_r of its imaginary part. With respect to R_r, because the sound pressure P_s and the vibration velocity $U_0e^{j\omega t}$ are in-phase, R_r contributes the acoustic radiation of plate 1. On the other hand, because P_s and $U_0e^{j\omega t}$ that relate to X_r have the phase shift of 90°, X_r does not take part in the acoustic radiation, whereas it functions in plate 1 as additional mass.

Because the natural frequency depends on the plate thickness although the radiation impedance is decided by its natura frequency and radius, here, the plate thickness is adopted as the influence parameter on the radiation impedance. Fig. 10 shows variations in the radiation resistance and reactance with the plate thickness h_c, however, the normalized R_{rn} and X_{rn} are adopted as a substitute for R_r and X_r. They increase with h_c, with the result that the rate of vibration energy that is directly spent on the acoustic radiation increases with h_c. Then because the additional mass means that the surrounding medium is involved in the plate vibration, the vibration energy is consumed further with increasing h_c. Therefore, the discrepancy between the theoretical and experimental P_{em} in Fig. 9 is caused by the acoustic radiation and additional mass and expands with increasing h_c due to the behaviors of the radiation resistance and reactance.

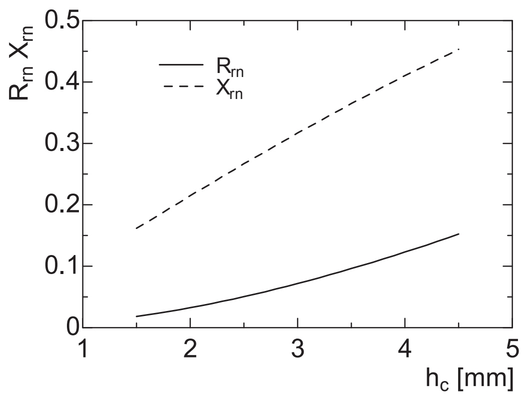

Fig. 10 Radiation resistance and reactance as function of plate thickness.

However, the piston source is different from the actual situation, so that it is hard that the above considerations are estimated quantitatively in that discrepancy. Hence the radiation impedance shold be reflected in the theoretical procedure to provide accurately the electricity generation efficiency.

5. Conclusion

In this study, the electricity generation system, which consisted of a circular plate installing a piezoelectric element at its center, was taken up. To improve that electricity generation characteristics by using the acoustic radiation energy derived from the plate vibration, the cylinder that has the above plates at both ends is adopted and the mechanical-acoustic coupling between the plate vibrations and internal sound field is used. Then the effect of mechanical-acoustic coupling on energy harvesting was estimated theoretically and experimentally from the electricity generation efficiency.

In the theoretical consideration, the electricity generation efficiency without coupling, i.e. by means of only the plate vibration, increases with the plate thickness. The efficiency with coupling, i.e. by means of the cylinder having both end plates, also increases with the plate thickness and behaves in the variation similar to that without coupling, so that the effect of coupling on the efficiency is hardly recognized. However, the experimental efficiency without coupling decreases with increasing the plate thickness and becomes the opposite tendency for the theory. As a result, a great discrepancy is confirmed between the theoretical and experimental efficiencies that are without coupling, while the effect of coupling on the efficiency is verified. Then the discrepancy is because the radiation impedance increases with the plate thickness and is not taken in consideration in the theoretical procedure.

Acknowledgement

This work was partially supported by JSPS KAKENHI Grant Number 15K05874.

References

1) S.R. Anton and H.A. Sodano: A review of power harvesting using piezoelectric materials (2003–2006), Smart Materials and Structures **16** No. 3, 1 (2007).
2) K. Yamada, H. Matsuhira and H. Utsuno: Improvement of efficiency of piezoelectric element attached to beam based on mechanical impedance matching, J. Sound Vib. **333** No. 1, 52 (2014).

3) M. Piñeirua, O. Doaré and S. Michelin: Influence and optimization of the electro desposition in a piezoelectric energy harvesting flag, J. Sound Vib. 346, 200 (2014).
4) J. Pan and D.A. Bies: The effect of fluid-structural coupling on sound waves in an enclosure - theoretical part, J. Acoust. Soc. Am. 87 No. 2, 691 (1990).
5) J. Pan and D.A. Bies: The effect of fluid-structural coupling on sound waves in an enclosure - experimental part, J. Acoust. Soc. Am. 87 No. 2, 708 (1990).
6) L. Cheng and J. Nicolas: Radiation of sound into a cylindrical enclosure from a point-driven end plate with general boundary conditions, J. Acoust. Soc. Am. 91 No. 3, 1504 (1992).
7) L. Cheng: Fluid-structural coupling of a plate-ended cylindrical shell: vibration and internal sound field, J. Sound Vib. 174 No. 5, 641 (1994).
8) K. Shiraki: Noise Prevention Design and Simulation (Applied Technology Publication) 1, 69 (1987).